Applied Catalysis B: Environmental 110 (2011) 141–147

Contents lists available at SciVerse ScienceDirect

Applied Catalysis B: Environmental

journal homepage: www.elsevier.com/locate/apcatb

PtSn/C alloyed and non-alloyed materials: Differences in the ethanol electro-oxidation reaction pathways

J.C.M. Silva [a,c], L.S. Parreira [a,c], R.F.B. De Souza [a,c], M.L. Calegaro [b,c], E.V. Spinacé [a,c], A.O. Neto [a,c], M.C. Santos [a,c,*]

[a] LEMN – Laboratório de Eletroquímica e Materiais Nanoestruturados, CCNH – Centro de Ciências Naturais e Humanas, UFABC – Universidade Federal do ABC, CEP 09.210-170, Rua Santa Adélia 166, Bairro Bangu, Santo André, SP, Brazil

[b] Grupo de Materiais Eletroquímicos e Métodos Eletroanalíticos, Instituto de Química de São Carlos, Universidade de São Paulo, Caixa Postal 780, 13566-590 São Carlos, SP, Brazil

[c] Instituto de Pesquisas Energéticas e Nucleares, IPEN, CNEN/SP, Av. Prof. Lineu Prestes, 2242 Cidade Universitária, CEP 05508-900, São Paulo, SP, Brazil

ARTICLE INFO

Article history:
Received 20 May 2011
Received in revised form 29 July 2011
Accepted 26 August 2011
Available online 3 September 2011

Keywords:
PtSn
Ethanol oxidation reaction
Alloyed materials

ABSTRACT

In the present work, the ethanol oxidation reaction (EOR) was investigated using PtSn/C electrocatalysts in the following two phases: 92% alloyed prepared by the polymeric precursor method (PPM) and 6% alloyed prepared by a sol–gel method (SGM). The TEM experiments show particle sizes of 3–5 nm for both catalysts. The electrocatalytic activity for both materials was investigated using chronoamperometry, and at 0.5 V vs. RHE, the current density for the EOR on the PPM material was approximately 5 times higher than on the SGM material. From *in situ* ATR-FTIR experiments, it can be seen that the non-alloyed materials led to CO_2 formation with slow kinetics, whereas alloyed materials led to acetic acid formation with fast kinetics. The enhancement in the electrocatalytic behavior for ethanol oxidation was explained by acetic acid formation.

1. Introduction

Direct ethanol fuel cells (DEFCs) have attracted great interest as alternative power sources in recent years [1–3]. Ethanol is one of the most promising fuels due to its low toxicity, high energy density and abundant availability, as well as the fact that it can be obtained easily from biomass [4–6].

Many studies have indicated that PtSn/C is the best catalyst for the ethanol oxidation reaction (EOR) in comparison with other Pt-based binary materials [1,7–15]. However, insight into the promoting effect of Sn on the activity of the Pt catalyst has been controversial. Discrepant viewpoints have focused on either the effects of either alloying Pt with Sn [9–11] or of combining it with SnO_2 [12–14]. Antolini et al. [7] reported good activity of $PtSnO_2$/C in a DEFC; however, in addition to a suitable $PtSnO_2$ ratio, a low degree of alloy is required to obtain a high EOR activity.

Zhu et al. [3] studied the effect that changing alloying degree in PtSn catalyst has on the catalytic behavior for ethanol electro-oxidation in DEFC. Of the three compositions studied, alloyed PtSn/C (54.9 and 14.4%) and non-alloyed $PtSnO_2$/C, the best result was obtained using PtSn/C with a higher alloy degree as anode catalyst on which the kinetics of the EOR was much faster than in the other cases. The worst result was obtained with the non-alloyed $PtSnO_2$/C catalyst.

Godoi et al. [9] reported that in the EOR, the performance of PtSn/C catalysts can be enhanced by an increase in the amount of alloyed phase at the expense of the oxides on the PtSn/C catalysts. De Souza et al. [16] reported that the Pt_3Sn/C alloy is a promising catalyst for ethanol oxidation. The performance of a DEFC was greatly improved when Pt_3Sn/C was used as the anode catalyst instead of a commercial PtSn/C E-TEK material. However, the authors reported that preparing binary PtSn alloys with a Pt_3Sn predominant phase is challenging.

Jiang et al. [17] studied how the product distributions generated from the EOR are affected as a function of binary PtSn/C catalysts' structural parameters. Using a $PtSnO_x$/C catalyst at different atomic ratios and online differential electrochemical mass spectroscopy (DEMS), they reported that the decrease of tin content favors acetic acid and acetaldehyde formation.

Indeed, the simultaneous utilization of auxiliary techniques and electrochemical methods to study the mechanism of small organic molecules electro-oxidation is one of the most powerful procedures to elucidate several aspects of these processes, including the influence of structural parameters of the catalyst on the reaction mechanism. In addition to the DEMS [17–20], other techniques can be used to study the mechanisms of the EOR with different electrocatalytic processes such as sum frequency generation

* Corresponding author at: LEMN – Laboratório de Eletroquímica e Materiais Nanoestruturados, CCNH – Centro de Ciências Naturais e Humanas, UFABC – Universidade Federal do ABC, CEP 09.210-170, Rua Santa Adélia 166, Bairro Bangu, Santo André, SP, Brazil. Tel.: +55 11 4996 0163; fax: +55 11 4437 8350.
E-mail address: mauro.santos@ufabc.edu.br (M.C. Santos).

0926-3373/$ – see front matter © 2011 Elsevier B.V. All rights reserved.
doi:10.1016/j.apcatb.2011.08.036

(SFG) [21], ellipsometry [22], Raman Spectroscopy [23,24], and the "*in situ*" Fourier Transform Infrared Spectroscopy (FTIR "*in situ*" Spectroscopy) [25–30].

Using the "*in situ*" FTIR, it is possible to study the EOR pathways and determine the product distributions at different potentials as a function of the PtSn/C catalyst structure and composition. In this study, the effects of alloyed and non-alloyed Pt:Sn phases on the EOR has been investigated using FTIR "*in situ*" spectroscopy in the ATR mode. Structural effects of alloyed and non-alloyed phases have been distinguished, correlating product selectivity and distribution via spectroscopic/electrochemical information.

2. Materials and methods

The PtSn electrocatalysts with a 3:1 mass ratio and 20 wt.% metal/carbon Vulcan XC-72R were prepared using two different methods. Alloyed material was prepared by the polymeric precursor method (PPM) as a described by De Souza et al. [16,24,31,32]. Briefly, the precursor solution was prepared by dissolving citric acid (CA) into ethylene glycol (EG) at a 50:400 molar ratio at 60 °C. $H_2PtCl_6{\cdot}7H_2O$ and $SnCl_2$ at a mass ratio Pt:Sn (3:1) were added to this solution while maintaining a molar ratio of 1:50:400 (metal:CA:EG). The catalysts were prepared by placing a predetermined volume of the resin in an appropriate amount of Vulcan XC-72R carbon (Cabot Corporation), followed by the addition of EG. These mixtures were homogenized in an ultrasonic bath for 60 min and thermally treated at 400 °C for 120 min under N_2 atmosphere.

Non-alloyed PtSn material was prepared using the sol–gel method [2]. Briefly, adequate amounts of Vulcan carbon XC72R, $H_2PtCl_6{\cdot}7H_2O$ and $SnCl_2$ were mixed together to obtain an electrocatalyst with a Pt:Sn mass ratio of (3:1) and 20% metal loading on carbon. Subsequently, appropriate amounts of isopropyl alcohol and acetic acid were added to this mixture. The final mixture was then homogenized in an ultrasonic bath for 30 min. Subsequently, the solvent was evaporated and the resulting powder was thermally treated at 400 °C for 120 min under flowing N_2.

XRD analyses were performed using a Rigaku diffractometer (model Multiflex) with a CuKα radiation source. Morphological information was obtained by the TEM technique via a FEI Tecnai G2 20 TEM instrument operating at 200 kV.

Electrochemical measurements were performed at room temperature using an Autolab PGSTAT 302N potentiostat. Glassy carbon (GC) electrodes were employed as a support for the working electrodes (0.07 cm^2 of geometric area). In a three-compartment electrochemical cell, a large Pt foil was used as a counter electrode. All potentials were referred to a reversible hydrogen electrode (RHE). Before each experiment, the GC support was polished with alumina suspension (1 μm) to a mirror finish and washed in a mixture of ethanol and water. Ultrapure water obtained from a Milli-Q system (Millipore®) was used in all experimental procedures.

The working electrodes were constructed by dispersing 8 mg of the electrocatalyst powder in 1 mL water and mixing for 5 min in an ultrasonic bath. Shortly thereafter, 20 μL of 5% Nafion® solution was added to the suspension, which was mixed again for 15 min in an ultrasonic bath. Aliquots of 4 μL of the dispersion fluid were pipetted onto the GC surface. Finally, the electrode was dried at 60 °C for 20 min and hydrated for 5 min in water. Chronoamperometric experiments were performed in a 0.5 mol L^{-1} H_2SO_4 solution containing 1 mol L^{-1} ethanol.

The spectroelectrochemical ATR-FTIR *in situ* measurements were performed with a Varian® 660 IR spectrometer equipped with a MCT detector cooled with liquid N_2, a MIRacle with a Diamond/ZnSe Crystal Plate (Pike®) ATR accessory and a special cell, as illustrated in Fig. 1.

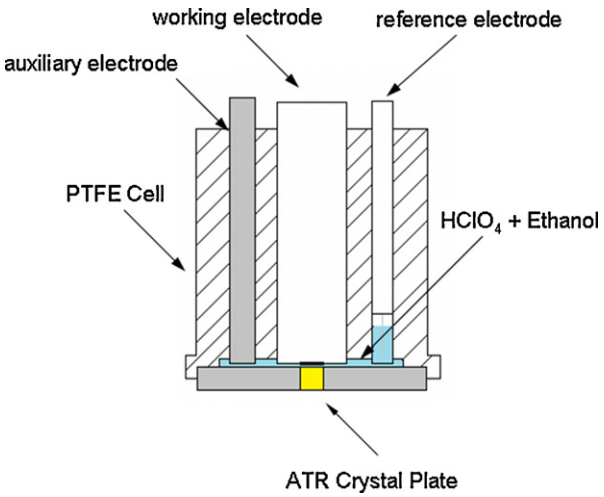

Fig. 1. Experimental arrangement for ATR-FTIR *in situ* setup.

The same working electrode used in the electrochemical experiments was also used in ATR-FTIR measurements. These experiments were performed at 25 °C in 0.1 mol L^{-1} $HClO_4$ containing 0.5, 1.0 and 2.0 mol L^{-1} ethanol. The absorbance spectra were collected as the ratio R:R_0, where R represents a spectrum at a given potential and R_0 is the spectrum collected at 0.05 V. Positive and negative directional bands represent gain and loss of species at the sampling potential, respectively. The spectra were computed from 128 interferograms averaged from 2500 cm^{-1} to 850 cm^{-1} with the spectral resolution set to 4 cm^{-1}. Initially, a reference spectrum (R_0) was measured at 0.05 V, and the sample spectra were collected after applying successive potential steps from 0.2 V to 1.0 V.

3. Results and discussion

Fig. 2 shows the XRD patterns for PtSn/C catalysts. The Pt peak positions (dashed lines) are also included for reference. The

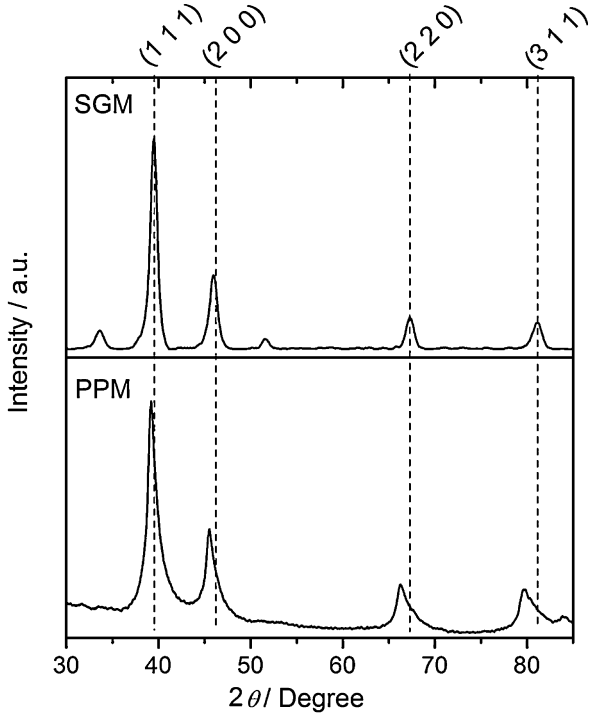

Fig. 2. X-ray diffraction patterns for PtSn/C electrocatalysts.

Table 1
Catalyst morphological information obtained from TEM images.

Electrocatalyst	Mean diameter (nm)	Standard deviation (nm)	Maximum diameter (nm)	Minimum diameter (nm)
Pt_3Sn/C PPM	5.1	1.8	10.9	2.6
$PtSnO_2$/C SGM	4.8	1.8	10.9	2.4

XRD patterns indicate that both materials present the same face-centered cubic (fcc) structure of platinum, with a shift in the peak positions for the lower 2θ values caused by a change in the lattice parameters due to the incorporation of Sn atoms [16]. For SGM, small signals that could be attributed to SnO_2 (JCPDF # 41-1445) can be observed at 2θ values around 33° and 51° [2]. However, the presence of tin oxides in the form of amorphous oxides cannot be discarded. The mean crystallite sizes estimated using Scherrer's equation were 5 nm for the PPM sample and 4.2 nm for the SGM catalysts.

The lattice parameters of the electrocatalysts were calculated from the Pt (2 2 0) peak position using Eq. (1) [14]

$$a_{(\mathrm{fcc})} = \frac{2^{1/2}\lambda_{k\alpha 1}}{\sin\theta} \quad (1)$$

where $a_{(\mathrm{fcc})}$ is the lattice parameter and $\lambda_{k\alpha 1}$ is the X-ray wavelength (1.54 Å). For PPM material is obtained a lattice parameter of 3.9942 Å and 3.9201 Å for the SGM material. Following a procedure described in the literature [16,33], the amount of alloyed Sn (f_{Sn}) in the Pt_3Sn/C PPM catalyst can be calculated using the relationship 2:

$$f_{\mathrm{Sn}} = \left[\frac{(a_c - a_o)}{(a_s - a_o)}\right] x_s \quad (2)$$

where a_c is the experimental lattice parameter calculated above, a_o = 3.9075 Å [34] is the lattice parameter of a Pt/C material with size (~4.5 nm) comparable to the size of the catalyst particles in the present work, a_s is the network parameter for Pt_3Sn/C (4.0015 Å, ca. 100% alloyed), and x_s is the Sn atomic fraction (0.25). Substituting the respective values into Eq. (2) yields values of 0.23 and 0.015 for f_{Sn}, respectively for PPM and SGM materials, indicating that of the 25% mass fraction of Sn originally used in the synthesis, 23% is present as Pt_3Sn/C on PPM material and 1.5% on SGM material. The findings above indicate that the PPM approach produces Pt3Sn/C 92% alloyed while SGM produces 6% alloyed.

Fig. 3 presents TEM micrographs and a histogram of the catalyst particle mean diameter distribution for Pt_3Sn/C PPM (Fig. 3a and b) and $PtSnO_2$/C SGM (Fig. 3c and d). In both cases, the particles were highly dispersed on the carbon support, although some small particle aggregates can be observed for Pt_3Sn/C PPM (Fig. 3a). The particles are with average sizes of 4.8 nm for SGM and 5.1 nm for

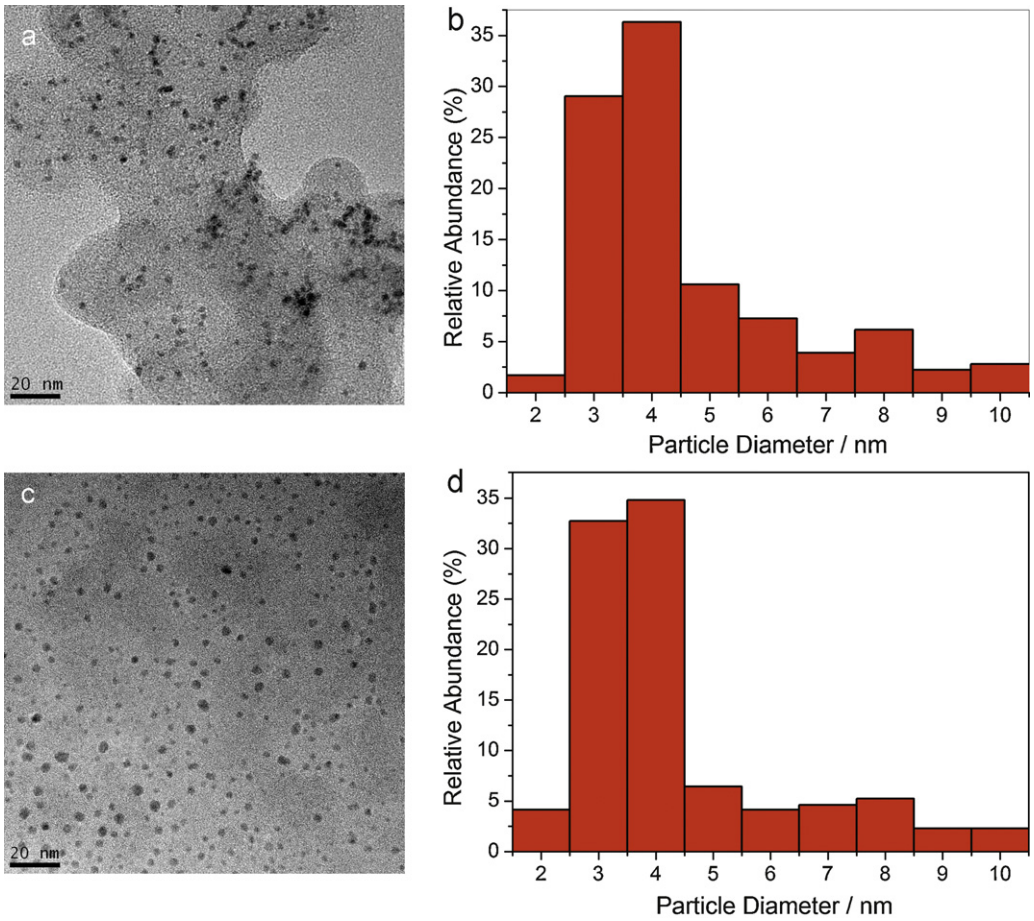

Fig. 3. (a) TEM micrograph of the PPM electrocatalyst; (b) histogram of catalyst particle mean diameter distribution for this electrocatalyst; (c) TEM micrograph of the SGM electrocatalyst; (d) histogram of the catalyst particle mean diameter distribution for this electrocatalyst.

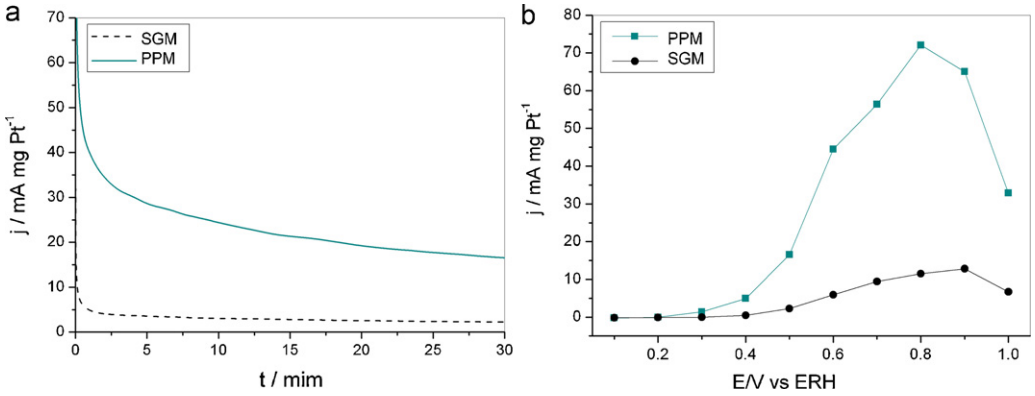

Fig. 4. (a) Chronoamperometry curves for the 20 wt.% PtSn/C electrocatalysts in 1.0 mol L^{-1} CH_3CH_2OH + 0.5 mol L^{-1} $HClO_4$. E = 0.5 V, time = 30 min, T = 25 °C. (b) Polarization curves for the 20 wt.% PtSn/C electrocatalysts in 1.0 mol L^{-1} CH_3CH_2OH + 0.5 mol L^{-1} $HClO_4$. Potential was polarized in a range from 0.1 V up to 1.0 V for 30 min in each potential and the current values on the graphic are the final currents at 30 min of the experiment.

the PPM materials. It should be noted that 100% of the particles are between 2 and 10 nm in size. Table 1 summarizes the mean, maximum and minimum sizes and the standard deviation of the catalyst particles estimated from the TEM images. These results are in agreement with both our previous studies [2,16] and with the work of Purgato et al. [35]. The TEM results are also in accordance with the mean crystallites sizes calculated from XRD data.

Fig. 4a shows the chronoamperometric curves for ethanol electro-oxidation on PtSn/C electrocatalysts obtained by polarization at 0.5 V for 30 min. Fig. 4b shows the results for ethanol electro-oxidation on PtSn/C obtained by chronoamperometric experiments in which the potential was polarized in a range from 0.1 V up to 1.0 V for 30 min in each potential and the current values on the graphic are the final currents at 30 min of the experiment. The measured current density for ethanol oxidation at 0.5 V on PPM material is the highest. Furthermore, ethanol oxidation reaction using PtSn/C MPP had the highest current densities above 0.2 V in all potentials. This result is in agreement with the work of Godoi et al. [9] and Zhu et al. [3], in which better activity for the EOR on PtSn/C catalysts were obtained for materials with a higher alloy degree. The EOR is faster on alloyed PtSn/C than on non-alloyed PtSn/C, as reported by Zhu et al. [3]. In their experiments, the best result for the EOR was obtained using the PtSn/C with a higher alloy degree. However, the results reported in this paper are at constant temperature of 25 °C, since as demonstrated for Gupta et al. [36] the temperature have effects on kinetics on ethanol electro-oxidation. To understand the differences in the kinetic of ethanol oxidation on the SGM and PPM materials, insight into the products generated is necessary.

Fig. 5 shows two sets of spectra measured for ethanol oxidation on PPM and SGM electrocatalysts. Bands corresponding to acetic acid (1280 cm^{-1}) [37], acetaldehyde (933 cm^{-1}) [29] and CO_2 (2343 cm^{-1}) [38] were measured. For the EOR on the SGM material, spectral IR bands for both CO_2 and acetaldehyde appear only at potentials higher than 0.4 V vs. RHE (0.1 V higher for the PPM material). The acetic acid bands can only be seen after 0.5 V (0.2 V higher for the PPM material). Other spectral bands can be observed at 1130, ~1630 and 1710 cm^{-1} for the PPM and SGM materials.

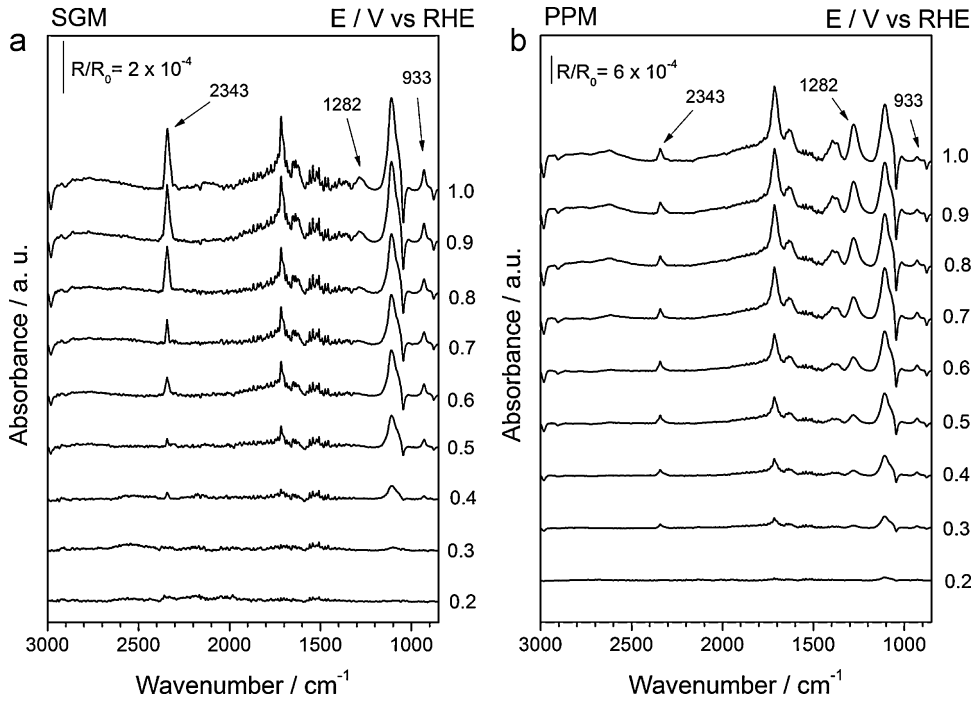

Fig. 5. The *in situ* FTIR spectra collected at several potentials for the EOR on PtSn/C SGM and PPM materials. Backgrounds collected at 0.05 V (RHE scale).

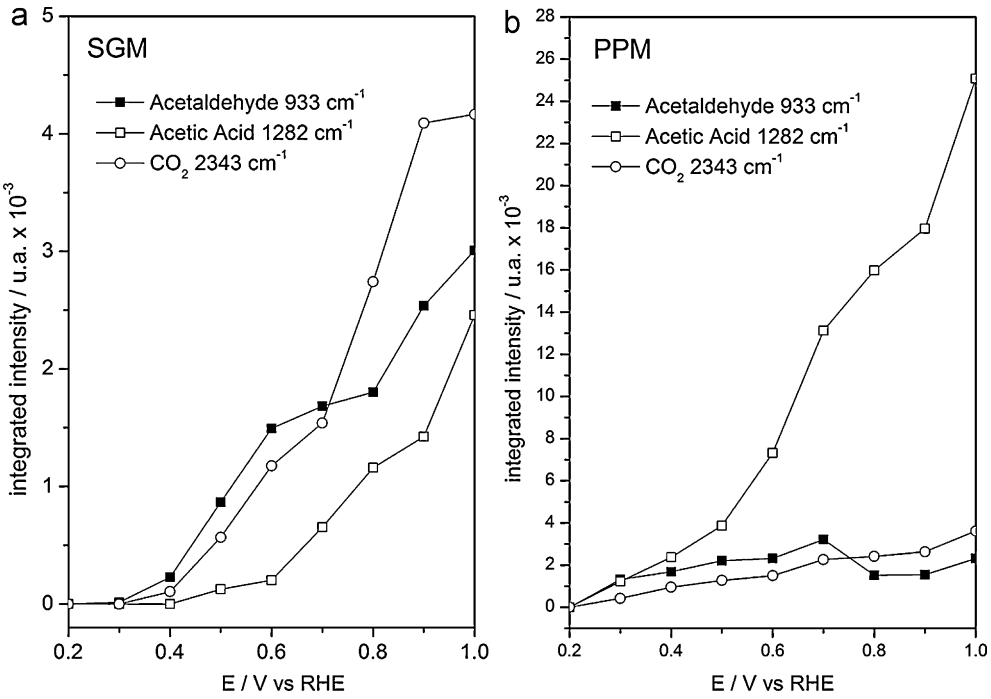

Fig. 6. Integrated CO_2, acetic acid and acetaldehyde band intensity as a function of the electrode potential for: (a) the SGM materials and (b) the PPM materials.

These bands may be ascribed to the triply degenerate ν_3 mode of adsorbed perchlorate anions, the HOH deformation, and the C = O stretch of the carbonyl group, respectively [39].

To evaluate the effect of catalyst structures on the product distribution during the EOR at different potentials, all bands were deconvoluted to Lorentzian line forms. Thus, the intensity and line width of each band could be individually analyzed. Fig. 6 presents the integrated intensity of the acetic acid, acetaldehyde and CO_2.

Fig. 6b shows that for the PPM material, acetic acid is the main product in the potential range studied as indicated by the integrated band intensities. For SGM, however, the acetaldehyde and CO_2 integrated band intensities are bigger than for the acetic acid. To assess a comparative relation among the electrocatalysts studied, the integrated band intensities for the CO_2/acetaldehyde and CO_2/acetic acid ratios as a function of the electrode potential have been examined. Those results are presented in Fig. 7.

The ratio bands of acetaldehyde and CO_2 are seen in Fig. 7a and are similar for both the PPM and SGM materials. From 0.3 to 0.7 V, the production of acetaldehyde is favored, and at higher potentials, the CO_2 production is the predominant path. This result suggests that the higher catalytic activity toward the EOR presented by the PPM material is related to the acetic acid production.

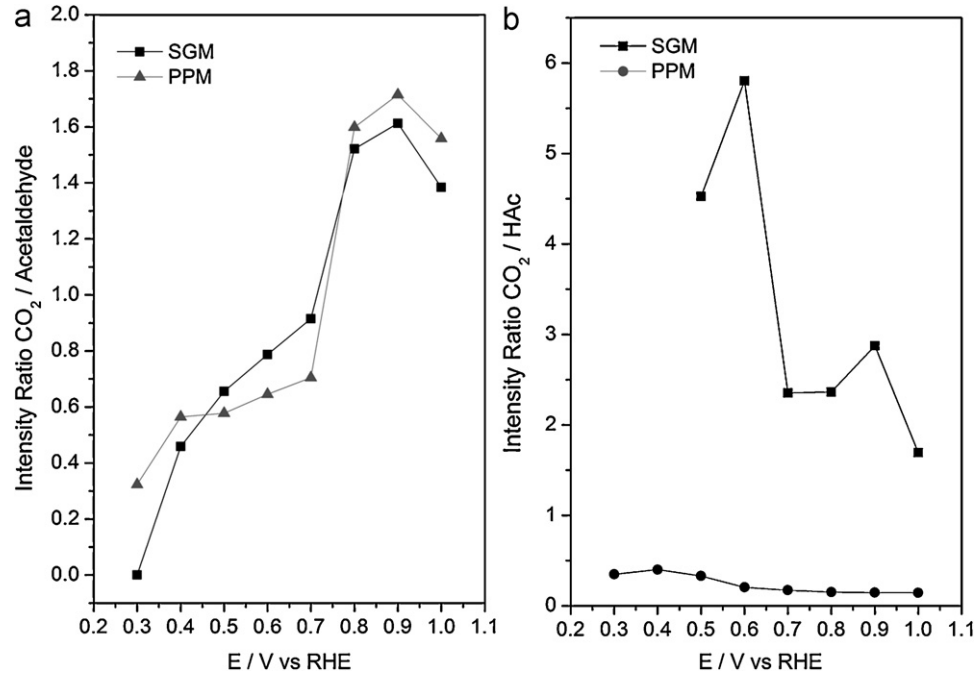

Fig. 7. Band intensity ratios of different products from the EOR on the SGM and the PPM materials (2 mol L^{-1} C_2H_5OH/0.1 mol L^{-1} $HClO_4$ solutions) as a function of the electrode potential: (a) CO_2/acetaldehyde band intensity ratio and (b) CO_2/acetic acid band intensity ratio.

On the one hand, the results show that for the EOR on the SGM material, a higher CO_2/acetic acid ratio (Fig. 7b) is obtained in all potential regions, indicating a preferential oxidation of ethanol to CO_2, as suggested by Lima and Gonzalez [40] (reaction proceeds preferably by the 12 electrons path). Alternatively, for the PPM material, the CO_2/acetic acid ratio is low, indicating that ethanol is converted mainly to acetic acid (the reaction occurs preferably by a 4-electron path). However, the kinetics of the EOR are faster on the PPM material than on SGM material, as observed in the chronoamperometric experiments.

The decrease in the CO_2/HAc ratio in the PPM catalysts is directly related to the catalyst structure. When Pt is alloyed with Sn, the Pt–Pt distance is increased, and the ability of Pt to dissociate the C–H bonds of the adsorbed ethanol molecules is inhibited as described by Gupta et al. [36]. The deactivation of ethanol C–H bonds favors the production of acetic acid. At this point, the kinetics of ethanol oxidation to acid acetic on an alloyed material is important. Zhu et al. [3] reported the fast kinetics of the EOR on PtSn/C with a high alloying degree. Ethanol adsorption is probably favored on $PtSnO_2$/C in comparison to Pt_3Sn/C, since Pt–Pt distance is not modified and Pt is well known for the adsorption of small organic molecules. In one hand, this detail can increase the possibility of C–C cleavage. On the other hand, the higher the ethanol adsorption the higher the poisoning by strongly bonded intermediates leading to a slow kinetic for EOR.

Our results for the EOR on $PtSnO_2$/C electrocatalysts are not in agreement with those reported by Jiang et al. [17], which indicate higher production of acetaldehyde and acetic acid using $PtSnO_x$/C. In their experiments, however, the catalysts were prepared with Pt:Sn atomic ratios of (5:5), (6:4), (7:3), and (8:2), with the Pt loading in each catalyst being 20 wt.% on carbon. In our study, the catalysts were prepared with a mass ratio of Pt:Sn (3:1) and 20 wt.% of metals on carbon. In the work of Jiang et al. [17], the product distribution from ethanol oxidation (1 mol L^{-1}) was evaluated by DEMS polarizing the electrode for 15 min in the potential range from 0.06 up to 0.6 V vs. RHE. In our study, we used the "*in situ*" ATR-FTIR and the product distribution for ethanol oxidation (0.5, 1 and 2 mol L^{-1}), which was evaluated after polarizing the electrode for just 30 s in each potential of a different interval (from 0.2 up to 1.0 V). In fact, a comparison with similar work is difficult because of the different physicochemical properties presented by the catalysts used in such studies. Materials prepared by a variety of methods present distinct properties, including composition, structure, morphology, particle size, and degree of alloying, all of which are strongly dependent on synthesis conditions, as reported by Godoi et al. [9]. In Jiang et al. studies [17], for the EOR on Pt/SnO_x/C, a larger amount of acetic acid is formed, and CO_2 formation contributes less than 2% of the oxidation currents using Pt/SnO_x/C. However, when the authors used the Pt_3Sn/C alloy E-TEK as a catalyst for the EOR, only traces of CO_2 were detected. From this point of view, our study is in agreement with Jiang et al. [16]. The CO_2 formation from the ethanol oxidation reaction on Pt_3Sn/C PPM is very low. In our study, we determined that acetic acid is formed to a greater extent on Pt_3Sn/C PPM in all potential regions. Furthermore, electrochemical experiments indicated that the current densities for EOR using an alloyed material were higher than were those ones using a non-alloyed material, in which the conversion to CO_2 is more pronounced. Non-alloyed electrocatalysts oxidize ethanol to CO_2, but the kinetics are slow, resulting in low current densities. It is important to stress that the results obtained regarding different electrocatalytic structures are for the materials used. When we consider Sn modifying Pt single crystals optimum C–C cleavage was observed to depend not only on the precise Sn coverage on Pt but also on Pt single crystal facet orientation [41].

Similar results to those presented in Fig. 7 have also been obtained for different ethanol concentrations. This is especially the case for 2 mol L^{-1} ethanol. At 0.5 V, the CO_2/acetic acid ratio for the EOR on the PPM material was 0.142, while the SGM was 5. Ethanol at 2 mol L^{-1} is usually the highest concentration observed in DEFC tests.

Single direct ethanol fuel cell tests using Pt_3Sn/C as the anode catalyst, similar to those reported here, were performed by De Souza et al. [16]. In that study, the best performance was measured for the alloyed material (maximum power density of 58 mW cm^{-2}). Zhu et al. [10] recently reported the results of single fuel cell tests using PtSn/C alloyed and non-alloyed materials. The lowest power density was obtained with the non-alloyed material ($PtSnO_2$/C). Our results suggest that the best results obtained on a DEFC using Pt_3Sn/C alloy are due to the acetic acid production.

4. Conclusions

This study found that materials with similar chemical composition and similar mean crystallite sizes (4.8 nm to SGM and 5.1 nm to the PPM material) but with different structures for the materials used have different activities in the EOR. Materials prepared by the polymeric precursors method presented an alloy degree of 92% (alloyed material), while SGM materials presented an alloy degree of 6% (non-alloyed material). The chronoamperometric experiments showed that higher ethanol electro-oxidation activity was obtained on the PPM material than on the SGM material. Different activities are associated with both intrinsic pathways and the kinetic parameters of each type of material used. On non-alloyed catalysts, the C–C bond breaking is favored, and a high conversion of ethanol to CO_2 is obtained. However, in this case, the kinetics are slow, and appreciable current is observed only at high potential values. For alloyed catalysts, acetic acid is preferentially formed with fast kinetics.

Acknowledgements

This work was supported by Fapesp (09/09145-6, 10/07831-7, 10/16511-6, 10/16511-6), UFABC, CAPES and CNPq (473308/2010-0).

References

[1] E. Antolini, Journal of Power Sources 170 (2007) 1–12.
[2] J.C.M. Silva, R.F.B. De Souza, L.S. Parreira, E.T. Neto, M.L. Calegaro, M.C. Santos, Applied Catalysis B: Environmental 99 (2010) 265–271.
[3] M. Zhu, G. Sun, Q. Xin, Electrochimica Acta 54 (2009) 1511–1518.
[4] R.N. Singh, A. Singh, Anindita, Carbon 47 (2009) 271–278.
[5] A. Kowal, M. Li, M. Shao, K. Sasaki, M.B. Vukmirovic, J. Zhang, N.S. Marinkovic, P. Liu, A.I. Frenkel, R.R. Adzic, Nature Materials 8 (2009) 325–330.
[6] S.G. Lemos, R.T.S. Oliveira, M.C. Santos, P.A.P. Nascente, L.O.S. Bulhões, E.C. Pereira, Journal of Power Sources 163 (2007) 695–701.
[7] E. Antolini, F. Colmati, E.R. Gonzalez, Journal of Power Sources 193 (2009) 555–561.
[8] F. Colmati, E. Antolini, E.R. Gonzalez, Applied Catalysis B: Environmental 73 (2007) 106–115.
[9] D.R.M. Godoi, J. Perez, H.M. Villullas, Journal of Power Sources 195 (2010) 3394–3401.
[10] M.Y. Zhu, G.Q. Sun, S.Y. Yan, H.Q. Li, Q. Xin, Energy & Fuels 23 (2009) 403–407.
[11] J.H. Kim, S.M. Choi, S.H. Nam, M.H. Seo, S.H. Choi, W.B. Kim, Applied Catalysis B: Environmental 82 (2008) 89–102.
[12] L. Zheng, L. Xiong, J. Sun, J. Li, S. Yang, J. Xia, Catalysis Communications 9 (2008) 624–629.
[13] Z. Liu, L. Hong, S.W. Tay, Materials Chemistry and Physics 105 (2007) 222–228.
[14] D.-H. Lim, D.-H. Choi, W.-D. Lee, H.-I. Lee, Applied Catalysis B: Environmental 89 (2009) 484–493.
[15] A.O. Neto, R.R. Dias, M.M. Tusi, M. Linardi, E.V. Spinacé, Journal of Power Sources 166 (2007) 87–91.
[16] R.F.B. De Souza, L.S. Parreira, D.C. Rascio, J.C.M. Silva, E. Teixeira-Neto, M.L. Calegaro, E.V. Spinace, A.O. Neto, M.C. Santos, Journal of Power Sources 195 (2010) 1589–1593.
[17] L. Jiang, L. Colmenares, Z. Jusys, G.Q. Sun, R.J. Behm, Electrochimica Acta 53 (2007) 377–389.
[18] J. Barranco, A.R. Pierna, Journal of Power Sources 169 (2007) 71–76.

[19] T. Seiler, E.R. Savinova, K.A. Friedrich, U. Stimming, Electrochimica Acta 49 (2004) 3927–3936.
[20] H. Wang, Z. Jusys, R.J. Behm, Journal of Power Sources 154 (2006) 351–359.
[21] J.F. Gomes, B. Busson, A. Tadjeddine, G. Tremiliosi-Filho, Electrochimica Acta 53 (2008) 6899–6905.
[22] L. Zhou, S. Günther, D. Moszynski, R. Imbihl, Journal of Catalysis 235 (2005) 359–367.
[23] B. Ren, X.Q. Li, C.X. She, D.Y. Wu, Z.Q. Tian, Electrochimica Acta 46 (2000) 193–205.
[24] R.F.B. De Souza, É. Neto, M. Calegaro, E. Santos, H. Martinho, M. dos Santos, Electrocatalysis 2 (2011) 28–34.
[25] J.-T. Li, Q.-S. Chen, S.-G. Sun, Electrochimica Acta 52 (2007) 5725–5732.
[26] V. Pacheco Santos, V. Del Colle, R.B. de Lima, G. Tremiliosi-Filho, Electrochimica Acta 52 (2007) 2376–2385.
[27] G.A. Camara, R.B. de Lima, T. Iwasita, Journal of Electroanalytical Chemistry 585 (2005) 128–131.
[28] J. Ribeiro, D.M. dos Anjos, K.B. Kokoh, C. Coutanceau, J.M. Léger, P. Olivi, A.R. de Andrade, G. Tremiliosi-Filho, Electrochimica Acta 52 (2007) 6997–7006.
[29] M. Li, A. Kowal, K. Sasaki, N. Marinkovic, D. Su, E. Korach, P. Liu, R.R. Adzic, Electrochimica Acta 55 (2010) 4331–4338.
[30] F. Vigier, C. Coutanceau, F. Hahn, E.M. Belgsir, C. Lamy, Journal of Electroanalytical Chemistry 563 (2004) 81–89.
[31] R.F.B. De Souza, A.E.A. Flausino, D.C. Rascio, R.T.S. Oliveira, E.T. Neto, M.L. Calegaro, M.C. Santos, Applied Catalysis B: Environmental 91 (2009) 516–523.
[32] A.S. Polo, M.C. Santos, R.F.B. de Souza, W.A. Alves, Journal of Power Sources 196 (2011) 872–876.
[33] F. Colmati, E. Antolini, E.R. Gonzalez, Journal of the Electrochemical Society 154 (2007) B39–B47.
[34] J.R.C. Salgado, E.R. Gonzalez, Ecletica Quimica 28 (2003) 77–85.
[35] F.L.S. Purgato, P. Olivi, J.M. Léger, A.R. de Andrade, G. Tremiliosi-Filho, E.R. Gonzalez, C. Lamy, K.B. Kokoh, Journal of Electroanalytical Chemistry 628 (2009) 81–89.
[36] S. Sen Gupta, S. Singh, J. Datta, Materials Chemistry and Physics 120 (2010) 682–690.
[37] J.M. Léger, S. Rousseau, C. Coutanceau, F. Hahn, C. Lamy, Electrochimica Acta 50 (2005) 5118–5125.
[38] G.A. Camara, T. Iwasita, Journal of Electroanalytical Chemistry 578 (2005) 315–321.
[39] S.C.S. Lai, S.E.F. Kleijn, F.T.Z. Öztürk, V.C. van Rees Vellinga, J. Koning, P. Rodriguez, M.T.M. Koper, Catalysis Today 154 (2010) 92–104.
[40] F.H.B. Lima, E.R. Gonzalez, Electrochimica Acta 53 (2008) 2963–2971.
[41] A.A. El-Shafei, M. Eiswirth, Surface Science 604 (2010) 862–867.